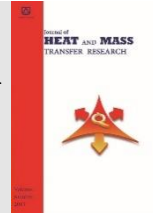




Semnan University



Numerical Analysis of Gas Flows in a Microchannel Applying the Cascaded Lattice Boltzmann Method with Varying Bosanquet Parameter

Morteza Shomali, Ahmad Reza Rahmati *

Department of Mechanical Engineering, University of Kashan, Kashan, 87317-51167, Iran,

PAPER INFO

Paper history:

Received: 2019-07-29

Revised: 2020-01-20

Accepted: 2019-11-29

Keywords:

Cascaded Lattice Boltzmann Method;
Micro Poiseuille Flows;
Boundary conditions;
Bosanquet parameter;
Effective viscosity.

ABSTRACT

In this study, a Cascaded Lattice Boltzmann Method with second-order slip boundary conditions is developed for inspecting gaseous flows in a microchannel in the slip and transition flow regimes with a wide range of Knudsen numbers. For the first time, the effect of wall confinement is deliberated on the effective mean free path of the gas molecules using a function with the nonconstant Bosanquet parameter as a substitute for the constant one. The constant-force driven and pressure-driven gas flows in a long microchannel are inquired under various conditions. The results of the velocity profile, pressure distribution, and flow rate are in good agreement with the benchmark solutions and experimental data in previous works. Further, the Knudsen minimum phenomenon is also well captured by the proposed model. The proposed Cascaded Lattice Boltzmann Method indicates a clear improvement in predicting the behavior of gaseous flows in microchannels for the previous classic and Cascaded Lattice Boltzmann Methods.

DOI: 10.22075/jhmtr.2020.18359.1243

© 2020 Published by Semnan University Press. All rights reserved.

1. Introduction

The process of building Microelectromechanical systems (MEMS) [1] referring to devices whose characteristic length is between 1 mm and 1 μ m, has greatly expanded recently. Therefore, the flow in microdevices receives more and more attention [2-4]. The microflows have a different mechanism from that of the macroscopic ones. In these flows, the order of characteristic length of the flow and the mean free path is the same.

Analytical solutions don't cover all the requirements of CFD applications when it comes to analyzing the microflow geometries. The Knudsen number (Kn) is a factor characterizing the microflows and defined as λ/H , where λ and H are the molecular mean free path and characteristic length, respectively. When $Kn > 0.01$, the Navier–Stokes equations are invalid, and some particular-based methods such as Molecular Dynamics and the Direct Simulation Monte Carlo are employed in numerical approaches [5-8]. However, these approaches are

computationally expensive. Recently, the researchers have paid significant attention to the lattice Boltzmann method (LBM) as a better approach [9-11].

The basis of the Lattice Boltzmann Method is the Lattice Boltzmann Equation with the BGK collision operator [12]. It contains two features. First, the collision between the wall and fluid particles is applied to the model via the mean free path. Second, the particles streaming is incorporated [5].

There are various theoretical and experimental models in the field of microflows that Beskok and Karniadakis categorized some of them in their work [10]. In accordance with Kn number, compressibility is another consequential parameter that reflects the fact that the pressure distribution is not linear in a microchannel. Basically, gas flows are compressible. Furthermore, in a long microchannel, a high-pressure difference is required to drive the fluid. Cercignani and Daneri [6] studied the poiseuille flow of a gas, numerically. The inverse Kn number range that they investigated was 0-10.5. Ohwada

*Corresponding Author: Ahmad Reza Rahmati, Department of Mechanical Engineering, University of Kashan, Kashan, 87317-51167, Iran, Email: ar_rahmati@kashanu.ac.ir

et al. [7] inspected the thermal poiseuille gaseous flow of rarefied gas in a microchannel. Their model was based on Linearized Boltzmann for Hard sphere molecules. The velocity distribution functions and gas heat flux was acquired in a spectrum range of Kn. Arkilic et al. [8] fabricated a microchannel for gaseous microflow. They displayed that a numerical method for compressible Navier-Stokes equations (NSE) with slip boundary conditions coordinates with the results of the fabricated microchannel. Hadjiconstantinou [9] concluded that modified second-order slip boundary conditions are compatible with the solution of the Boltzmann Equation for hard-sphere molecule for a wider spectrum of rarefaction.

Viscous heating and thermal creep are other major effects on microgrids [10, 11]. Ahmed and Beskok [12] explored the effects of viscous heating and rarefaction for microflows in microdevices. The slip velocity was the final important effect in gas microchannels.

Lee and Lin [13] inspected the slip velocity in the wall from the results of the simulation of the Lattice Boltzmann Method as a numerical error generated by the instability of the applied boundary conditions. However, it was clear that this slip velocity is a phenomenon present in the actual physics of microflows. Guo et al. [14] Systematically studied the symmetry, accuracy, and relaxation coefficient of the LBM for the microflows for Kn numbers from 0.1 and 10. They manifested that the symmetry and accuracy of the common Lattice Boltzmann Methods cannot simulate gaseous microflows in the transition state well. Moreover, in the gaseous microflows, the channel wall enclosure has nonlinear effects on the relaxation coefficient which must be deliberated in the LBM to model these flows.

Recently, Asadollahi et al. [15] explored the condensation process, the dynamic behavior of fluid, and phase-change inside a mini channel in the presence of square blocks, numerically. They employed multiphase LBM based on the pseudopotential model. In another study, Asadollahi et al. [16] removed the condensed liquid from an object and studied how wet is the surface in multiphase flows by Lattice Boltzmann Method. Hosseini et al. [17] studied a radiation and convection heat transfer problem in a microchannel with LBM. Their models agreed well with previous results.

Cascaded Lattice Boltzmann method (CLBM) eliminates modeling artifacts using a set of collision operators to simulate flows [18]. It improves the stability of the LBM for high Re numbers.

Several papers investigate the central moments and their high orders for the relaxation process in cascaded models [19-21]. They compare their CLBM models with some analytical solutions. Premnath and Banerjee [22] incorporated forcing terms in CLBM by a method of central moments. They concluded that their method is consistent with the NSE. They validated it with some benchmark problems. Fei and Lou also proposed another so-called Consistent forcing scheme in the CLBM that did

not apply orthogonal relaxation times [23]. The CLBM also is employed in some multiphase problems [24-26].

There is a lack of systematic study of numerical properties of gas flows in a microchannel for a wider spectrum of Kn number applying CLBM. This paper investigates flows in microdevices with CLBM and indicates the validation and efficiency of this method for the entire range of Kn numbers in various forms of microflows.

Here the LBM model will be discussed briefly, including a discussion about the LBM and the CLBM model for microflows In Section 2. Section 3 will inspect various wall-distance functions and incorporate them into boundary conditions. In Section 4, the CLBM for the microflows will be discussed. Section 5 will propose numerical results in detail and analyze them, and Section 6 gives a summary and conclusion of the present work.

2. The Lattice-Boltzmann Method

The recently applied LBM models are proposed by Bhatnagar et al. [27] called the BGK-Boltzmann. The discretized form of this equation in momentum, space, and time is as below:

$$f_i(\mathbf{x} + \mathbf{e}_i \delta t, t + \delta t) = f_i(\mathbf{x}, t) - \frac{\delta t}{\tau_s} (f_i(\mathbf{x}, t) - f_i^{eq}(\mathbf{x}, t)) \quad (1)$$

Where f_i , f_i^{eq} , c_i and τ_s are the discrete particle distribution function, equilibrium distribution function, velocity field, and the relaxation time, respectively. For the D2Q9 model used here, $\mathbf{e}_i = [|\mathbf{e}_{ix}\rangle, |\mathbf{e}_{iy}\rangle]$ is:

$$\begin{aligned} |\mathbf{e}_{ix}\rangle &= [0, 1, 0, -1, 0, 1, -1, -1, 1]^T \\ |\mathbf{e}_{iy}\rangle &= [0, 0, 1, 0, -1, 1, 1, -1, -1]^T \end{aligned} \quad (2)$$

Where $i=0-8$ and $|\cdot\rangle$ refers to a vector, and superscript T stands for transposition. Equation 2 relates the relaxation time (ν) to the fluid viscosity through the relation below:

$$\nu = c_s^2 \delta t (\tau_s - 0.5) \quad (3)$$

Where δt is the discrete time step and the sound speed $c_s = \frac{1}{\sqrt{3}} c$ in D2Q9 lattice and $c = \frac{\delta x}{\delta t}$. When the distribution functions are determined, the macroscopic properties like density (ρ), velocity vector (u) and pressure (P) would be computed applying relations below:

$$\rho = \sum_{i=0}^k f_i, \rho u = \sum_{i=0}^k \mathbf{e}_i f_i, P = c_s^2 \rho = \frac{1}{3} \rho \quad (4)$$

The equilibrium distribution functions is as below:

$$f_i^{eq} = w_i \rho \left(1 + 3 \frac{\mathbf{e}_i \cdot \mathbf{u}}{c_s^2} + \frac{9}{2} \frac{(\mathbf{e}_i \cdot \mathbf{u})^2}{c_s^4} - \frac{3}{2} \frac{u^2}{c_s^2} \right) \quad (5)$$

$$w_0 = 4/9, w_{i=1,2,3,4} = 1/9, w_{i=5,6,7,8} = 1/36$$

3. Wall-distance functions

The kinetic theory says the mean free path (λ) is related to the viscosity (μ) as [28, 29]

$$\lambda = \frac{\mu}{p} \sqrt{\frac{\pi RT}{2}} \quad (6)$$

Where T represents temperature. Equation (6) is true for rarefied gas flows in unbounded systems. Wall effects

are of the most important flow parameters, especially in the transition region. The collisions between walls and molecules are increasingly occurring, effectively reducing the gas mean free path [30].

For a micro gaseous flow between solid walls, the presence of walls has a great impact on the mean free path of the molecules. Various wall-distance functions [1, 29, 31] are proposed to record the effects of solid gas impact on flow properties. The general form of these functions can be expressed as below

$$\lambda^* = \lambda\Psi(Kn) \tag{7}$$

Where λ^* is the mean free path of the molecules in the confined system and Ψ is a function of Kn and distance from walls, and satisfying [14]

$$\lim_{Kn \rightarrow 0} \Psi(Kn) = 1 \tag{8}$$

The key parameter in the microflows is the relaxation parameter (τ_s), a collisional relaxation time scale to the local equilibrium, which appears in the BGK model for a collision operator. Pursuant to the relation between the viscosity and mean free path of the molecules, it can be concluded to

$$\mu_e = \mu\Psi(Kn) \tag{9}$$

where μ_e is the effective viscosity in the confined system. According to Equations (6) and (7), the effective viscosity μ_e can be acquired as:

$$\begin{aligned} \mu_e &= \frac{\rho}{3} \sqrt{\frac{2}{\pi RT}} \lambda^* = \frac{1}{3} \sqrt{\frac{6}{\pi}} \rho \lambda \Psi \\ &= \frac{c}{3} \sqrt{\frac{6}{\pi}} \rho N_y Kn \Psi \delta_x \end{aligned} \tag{10}$$

Where N_y represents the size of grid in the y-direction, and δx is the discrete lattice spacing. Therefore, using equation (3) and $\mu = \rho\vartheta$ we can obtain an expression for τ_s :

$$\tau_s = \sqrt{\frac{6}{\pi}} N_y Kn \Psi + \frac{1}{2} \tag{11}$$

The Knudsen number for poiseuille gas flows in a microchannel can be defined as below:

$$Kn = Kn_{out} P_{out} / P(x) \tag{12}$$

where Kn_{out} and P_{out} is the Knudsen number and outlet pressure.

3.1. Bosanquet-type effective viscosity

The Bosanquet-type effective viscosity is introduced by an interpolation formula proposed by Bosanquet for diffusion coefficients. It can be expressed as [10, 32]

$$\Psi = \frac{1}{1 + aKn} \tag{13}$$

where a is the Bosanquet parameter. Michalis *et al.* [32] used DSMC to study the rarefaction effect on viscosity for channel flows over the entire transition flow regime. Figure 1 shows their DSMC results in a channel for variation of the Bosanquet parameter with the Knudsen number. Each data set represents separated results with different end pressure values. They mentioned this dependence is relatively weak for most of the Kn numbers

in this region and shows an effective value of about 2. The majority of previous studies [31, 33] that employed Bosanquet-type effective viscosity, used this value. Some other values, such as 1.5 [9] and 2.2 [3, 10] were reported in the literature.

According to Figure 1, it can be observed that despite Michalis *et al.* suggestion, the dependence of the Bosanquet parameter with the Knudsen number is not weak, certainly for $Kn < 0.5$. In this paper, we suggest applying the nonconstant Bosanquet parameter instead of a constant one. After curve-fitting with various polynomial and arctangent-type functions, the best function that fits data over the whole range of Kn obtained as

$$a = 0.9586 + (2/\pi)arctan(39.27Kn^{2.613}) \tag{14}$$

Figure 1 also provides a comparison of the aforementioned suggestions for the constant Bosanquet parameter, including $a=1.5, 2, 2.2$, and the proposed model. It can be observed that the model proposed here fits data the best in comparison with the other models. The R-squared value of the curve-fitting is 0.08725; in spite of the shape of the curve proves its ability to fit the data. These values for $a=1.5, 2$ and 2.2 are $-3.614, -0.1014$ and -1.455 . In addition, the best exponential fitting function is $a = 1.935 \times \exp(-0.001221Kn) + 1.76 \times 10^{-13} \times \exp(1.484 \times Kn)$ that has R-squared value of 0.0129. Certainly, the arctangent-type function suggested here has the best prediction of the behavior of the data for $Kn < 0.5$. Although, the other models do not approximate the data in this region well.

Confirming to Equation 13, the Bosanquet parameters for different values of Kn such as 0.0194, 0.194, 0.388, 0.5 and 1 are 0.96, 1.27, 1.78, 1.86 and 1.94, respectively. These values of Kn are often applied in the literature for comparison with the analytical and experimental results. Table 1 provides the errors between the values of the proposed model and the other models discussed here. It can be interpreted that the errors of the previous models are not negligible, certainly for $Kn < 0.5$. For example, for $Kn = 0.0194$, the error for the most conventional model ($a=2$) is 108%, which is considerably large and can affect

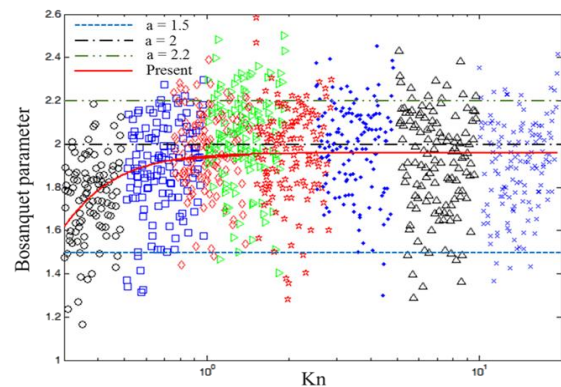


Figure 1. Variation of various models for the Bosanquet parameter with the Knudsen number. Data sets are from DSMC calculations [20]

the results of simulations for micro gas flows. Therefore, in this paper, Equation 13 is applied for the nonconstant Bosanquet parameter in the simulations.

3.2. Tang's function

Tang *et al.* [34] showed that the local mean free path of molecules of a gaseous flow between two walls, near the south wall, is represented as

$$\lambda_-(z) = \lambda_0(1 + (\alpha_1 - 1) \exp(-\alpha_1) - \alpha_1^2 E_i(\alpha_1)) \quad (15)$$

Where z is the direction normal to the wall, λ_0 is the reference mean free path, $\alpha_1 = z/\lambda_0$, $E_i(x) = \int_1^\infty t^{-1} e^{-xt} dt$

The local mean free path of molecules moving towards the upper wall can be written as:

$$\lambda_+(z) = \lambda_0(1 + (\alpha_2 - 1) \exp(-\alpha_2) - \alpha_2^2 E_i(\alpha_2)) \quad (16)$$

Where $\alpha_2 = (H-z)/\lambda_0$. The effective mean free path can be determined by averaging both of aforementioned mean free paths as:

$$\lambda = \frac{\lambda_+ + \lambda_-}{2} \quad (17)$$

3.3. Lockerby's function

Lockerby *et al.* [35] obtain a geometry-dependent expression of effective local viscosity. They proposed a function as below:

$$\Psi = \frac{1}{1 + 0.7 \exp(-Cz/\lambda)} \quad (18)$$

Where z is the distance normal to the wall and C is a constant that depends on the governing equations. Zhang *et al.* [36] showed that $C = 1$ is the best value that matches the results of the linearized Boltzmann equation and DSMC simulations.

3.4. Normalized effective mean free path function

Lopez [30] combined amplitude and profile to develop the Normalized effective mean free path function. The amplitude function is based on the molecular dynamics data at the center of the channel ($y/H=0.5$), plotted as a function of $1/Kn$. For the profile function, the reference data for each Kn is divided by the value at the center of the channel. Combining these functions gives the normalized effective mean free path function which can be written as:

$$\Psi \left(\frac{1}{Kn}, \frac{y}{H} \right) = \left(\frac{\left(\frac{1}{Kn} \right)^2 - 0.06 \left(\frac{1}{Kn} \right) + 0.38}{\left(\frac{1}{Kn} \right)^2 + 1} \right) \left(\frac{\left(\frac{y}{H} \right)^3_{\tan} + 0.53}{\left(\frac{y}{H} \right)^3_{\tan} + 1} \right) \quad (19)$$

3.5. Arctangent function

Stops [37] inspected the transition from continuum to molecular behavior of gases applying a modified mean free path. His expression of Ψ for a gas flow system confined between two parallel walls was very

Table 1. Percentage errors of various models for the Bosanquet parameter for different values of Kn

Kn	0.0194	0.194	0.388	0.5	1
a=1.5	56.4	17.8	15.4	19.4	22.8
a=2	108.5	57.1	12.9	7.5	3.0
a=2.2	129.3	72.8	24.2	18.3	13.3

complicated. Guo *et al.* [14] have approximated the function with:

$$\Psi = \frac{2}{\pi} \arctan(\sqrt{2}Kn^{-3/4}) \quad (20)$$

Finally. In this paper, the Bosanquet-type effective viscosity is chosen for modeling wall-distance effects.

4. The Cascaded Lattice Boltzmann Method

CLBM refers to a set of collision operator that decrease numerical instabilities. In the MRT model, the collision process is performed in a reference frame of a fixed lattice; however, in CLBM, this frame of reference is shifted by the macroscopic fluid velocity [6]. The local hydrodynamic velocity which is the first moment of the distribution functions, is the center of mass in the space of moments. The moments displaced by the local hydrodynamic velocity are central moments and defined in a reference frame moving with the fluid. Then again, the raw moments defined in the reference frame of a fixed lattice. The central moment of a given order is algebraic combinations of raw moments of dissimilar orders, with their highest order being equal to that of the central moment [38].

4.1. The Algorithm of Cascaded Lattice Boltzmann Method

The raw and central velocity moments of the distribution function are defined as:

$$\dot{\kappa}_{x^m y^n} = \sum_i f_i e_{ix}^m e_{iy}^n = \langle e_{ix}^m e_{iy}^n | f_i \rangle \quad (21)$$

$$\kappa_{x^m y^n} = \langle (e_{ix} - u_x)^m (e_{iy} - u_y)^n | f_i \rangle \quad (22)$$

Respectively, where f_i refers to discrete distribution functions and u_x and u_y are bulk velocities [23]. First, the lattice Boltzmann equation with a semi-implicit treatment of the forcing term is written as:

$$f_i(\mathbf{x} + \mathbf{e}_i \delta t, t + \delta t) = f_i(\mathbf{x}, t) + \Omega_i^C |_{(\mathbf{x}, t)} + \frac{\delta t}{2} (S_i |_{(\mathbf{x}, t)} + S_i |_{(\mathbf{x} + \mathbf{e}_i \delta t, t + \delta t)}) \quad (23)$$

where S_i is the forcing accounting for a body force field $F = (F_x, F_y)$ and Ω_i^C is the collision term which can be defined as:

$$\Omega_i^C = \Omega_i^C(f, \hat{g}) = (K \cdot \hat{g})_i \quad (24)$$

where $\hat{g} = |\hat{g}_i\rangle = (\hat{g}_0, \hat{g}_1, \hat{g}_2, \dots, \hat{g}_8)^T$ is the vector of the unknown collision kernels and \mathbf{K} is an orthogonal matrix defined as:

$$K = [|1\rangle, |e_x\rangle, |e_y\rangle, 3|e_x^2 + e_y^2\rangle, -4|1\rangle, |e_x^2 - e_y^2\rangle, |e_x e_y\rangle, -3|e_x^2 e_y\rangle + 2|e_y\rangle - 3|e_x e_y^2\rangle + 2|e_x\rangle, 9|e_x^2 e_y^2\rangle - 6|e_x^2 + e_y^2\rangle + 4|1\rangle] \quad (25)$$

The forcing term $S = |S_i\rangle = T^{-1}\hat{S}$, in which $\hat{S} = |\hat{S}_i\rangle$ can be written as:

$$\hat{S} = [0, \rho F_x, \rho F_y, 2\rho(F_x u_x + F_y u_y), 2\rho(F_x u_x - F_y u_y), \rho(F_x u_y + F_y u_x), \rho(F_y u_x^2 + 2F_x u_x u_y), \rho(F_x u_y^2 + 2F_y u_x u_y), \rho(2F_x u_x u_y^2 + 2F_y u_y u_x^2)]^T \quad (26)$$

T is a non-orthogonal transformation matrix which can be written as:

$$T = [|1\rangle, |e_x\rangle, |e_y\rangle, |e_x^2 + e_y^2\rangle, |e_x^2 - e_y^2\rangle, |e_x e_y\rangle, |e_x^2 e_y\rangle, |e_x e_y^2\rangle, |e_x^2 e_y^2\rangle]^T \quad (27)$$

The implicit treatment of the forcing term in Equation (23) makes its implementation in simulations complicated. By introducing a new distribution function $\tilde{f}_i = f_i - 0.5\delta t S_i$ the implicitness of this scheme can be avoided, which yields:

$$\tilde{f}_i(\mathbf{x}, t) = \tilde{f}_i(\mathbf{x}, t) + \Omega_i^C |_{(\mathbf{x}, t)} + \delta t S_i |_{(\mathbf{x}, t)} \quad (28)$$

$$\tilde{f}_i(\mathbf{x} + \mathbf{e}_i \delta t, t + \delta t) = \tilde{f}_i(\mathbf{x}, t) \quad (29)$$

Equations (28) and (29) represent collision and streaming step, respectively, and \tilde{f}_i is the post-collision distribution function.

It is noteworthy to mention that collisions do not alter mass and momenta. Considering the effect of the external force, the collision kernels $\hat{g} = |\hat{g}_i\rangle$ employing the expressions for discrete raw moments acquired as follows:

$$\hat{g}_0 = \hat{g}_1 = \hat{g}_2 = 0 \quad (30)$$

$$\hat{g}_3 = \frac{s_3}{12} \left\{ -(\hat{k}_{xx} + \hat{k}_{yy}) + \frac{2}{3}\rho + \rho(u_x^2 + u_y^2) - \frac{1}{2}\rho(2F_x u_x + 2F_y u_y) \right\} \quad (31)$$

$$\hat{g}_4 = \frac{s_4}{4} \left\{ -(\hat{k}_{xx} - \hat{k}_{yy}) + \rho(u_x^2 - u_y^2) - \frac{1}{2}\rho(2F_x u_x - 2F_y u_y) \right\} \quad (32)$$

$$\hat{g}_5 = \frac{s_5}{4} \left\{ -\hat{k}_{xy} + \rho u_x u_y - \frac{1}{2}\rho(F_x u_y + F_y u_x) \right\} \quad (33)$$

$$\hat{g}_6 = \frac{s_6}{4} \left\{ \hat{k}_{xxy} - 2u_x \hat{k}_{xy} - u_y \hat{k}_{xx} + 2\rho u_x^2 u_y - \frac{1}{2}\rho(F_y u_x^2 + 2F_x u_x u_y) - 2u_x \hat{g}_5 - \frac{1}{2}u_y(3\hat{g}_3 + \hat{g}_4) \right\} \quad (34)$$

$$\hat{g}_7 = \frac{s_7}{4} \left\{ \hat{k}_{xyy} - 2u_y \hat{k}_{xy} - u_x \hat{k}_{yy} + 2\rho u_x u_y^2 - \frac{1}{2}\rho(F_x u_y^2 + 2F_y u_x u_y) - 2u_y \hat{g}_5 - \frac{1}{2}u_x(3\hat{g}_3 - \hat{g}_4) \right\} \quad (35)$$

$$\hat{g}_8 = \frac{s_8}{4} \left\{ -[\hat{k}_{xxyy} - 2u_x \hat{k}_{xyy} - 2u_y \hat{k}_{xxy} + u_x^2 \hat{k}_{yy} + u_y^2 \hat{k}_{xx} + 4u_x u_y \hat{k}_{xy}] + \frac{1}{9}\rho + 3\rho u_x^2 u_y^2 - \frac{1}{2}\rho(2F_x u_x u_y^2 + 2F_y u_y u_x^2) - \frac{1}{2}u_x^2(3\hat{g}_3 - \hat{g}_4) - \frac{1}{2}u_y^2(3\hat{g}_3 + \hat{g}_4) - 4u_x u_y \hat{g}_5 - 2u_y \hat{g}_6 - 2u_x \hat{g}_7 \right\} - 2\hat{g}_3 \quad (36)$$

where $\{s_i | i = 3, 4, \dots, 8\}$ are relaxation parameters in the moment space. The discrete raw moments can be written as:

$$\hat{k}_0 = \rho \quad (37)$$

$$\hat{k}_x = \rho u_x - \frac{1}{2}\rho F_x \quad (38)$$

$$\hat{k}_y = \rho u_y - \frac{1}{2}\rho F_y \quad (39)$$

$$\hat{k}_{xx} = f_1 + f_3 + f_5 + f_6 + f_7 + f_8 \quad (40)$$

$$\hat{k}_{yy} = f_2 + f_4 + f_5 + f_6 + f_7 + f_8 \quad (41)$$

$$\hat{k}_{xy} = f_5 - f_6 + f_7 - f_8 \quad (42)$$

$$\hat{k}_{xxy} = f_5 + f_6 - f_7 - f_8 \quad (43)$$

$$\hat{k}_{xyy} = f_5 - f_6 - f_7 + f_8 \quad (44)$$

$$\hat{k}_{xxyy} = f_5 + f_6 + f_7 + f_8 \quad (45)$$

The kinematic viscosity (ϑ) and bulk viscosity (ζ) are given by:

$$\vartheta = c_s^2 \left(\frac{1}{s_\vartheta} - \frac{1}{2} \right) \delta t \quad (46)$$

$$\zeta = c_s^2 \left(\frac{1}{s_b} - \frac{1}{2} \right) \delta t \quad (47)$$

Respectively, where $s_4 = s_5 = s_\vartheta$ and $s_3 = s_b$ are the relaxation rate associated with shear viscosity and bulk viscosity, respectively. $s_6 = s_7 = s_q$, and s_8 are relaxation rates of the third and fourth-order moments which can be tuned independently of shear viscosity, and then brings an increase in stability. Equating all the relaxation rates to s_ϑ would decrease the CLBM scheme to LBGK. As a result of cascaded nature of the central moment approach, the collision kernel \hat{g}_i can be written as $\hat{g}_i = \hat{g}_i(f, \hat{g}_\beta)$, $\beta = 0, 1, i - 1$. Therefore, the evolution of lower-order raw moments influences higher-order central moments and not vice versa. Thus, starting from the lowest central moment, the higher-order central

moments can be relaxed successively towards their equilibrium, which is implicitly carried out in terms of raw moments [38]. The so-called "cascaded" collision naming is due to the aforementioned procedure.

Performing the cascaded collision, using matrix K the final distribution functions can be acquired as follows:

$$\tilde{f}_0 = \bar{f}_0 + [\hat{g}_0 - 4(\hat{g}_3 - \hat{g}_8)] + \delta t S_0 \quad (48)$$

$$\tilde{f}_1 = \bar{f}_1 + [\hat{g}_0 + \hat{g}_1 - \hat{g}_3 + \hat{g}_4 + 2(\hat{g}_7 - \hat{g}_8)] + \delta t S_1 \quad (49)$$

$$\tilde{f}_2 = \bar{f}_2 + [\hat{g}_0 + \hat{g}_2 - \hat{g}_3 - \hat{g}_4 + 2(\hat{g}_6 - \hat{g}_8)] + \delta t S_2 \quad (50)$$

$$\tilde{f}_3 = \bar{f}_3 + [\hat{g}_0 - \hat{g}_1 - \hat{g}_3 + \hat{g}_4 + 2(\hat{g}_7 + \hat{g}_8)] + \delta t S_3 \quad (51)$$

$$\tilde{f}_4 = \bar{f}_4 + [\hat{g}_0 - \hat{g}_2 - \hat{g}_3 - \hat{g}_4 - 2(\hat{g}_6 + \hat{g}_8)] + \delta t S_4 \quad (52)$$

$$\tilde{f}_5 = \bar{f}_5 + [\hat{g}_0 + \hat{g}_1 + \hat{g}_2 + 2\hat{g}_3 + \hat{g}_5 - \hat{g}_6 - \hat{g}_7 + \hat{g}_8] + \delta t S_5 \quad (53)$$

$$\tilde{f}_6 = \bar{f}_6 + [\hat{g}_0 - \hat{g}_1 + \hat{g}_2 + 2\hat{g}_3 - \hat{g}_5 - \hat{g}_6 + \hat{g}_7 + \hat{g}_8] + \delta t S_6 \quad (54)$$

$$\tilde{f}_7 = \bar{f}_7 + [\hat{g}_0 - \hat{g}_1 - \hat{g}_2 + 2\hat{g}_3 + \hat{g}_5 + \hat{g}_6 + \hat{g}_7 + \hat{g}_8] + \delta t S_7 \quad (55)$$

$$\tilde{f}_8 = \bar{f}_8 + [\hat{g}_0 + \hat{g}_1 - \hat{g}_2 + 2\hat{g}_3 - \hat{g}_5 + \hat{g}_6 - \hat{g}_7 + \hat{g}_8] + \delta t S_8 \quad (56)$$

Finally, the macroscopic properties would be determined through the relations below:

$$\rho = \sum_{i=0}^k \tilde{f}_i, \rho u = \sum_{i=0}^k \mathbf{e}_i \tilde{f}_i + \frac{\delta t}{2} \rho \mathbf{F}, \quad (57)$$

$$P = c_s^2 \rho = \frac{1}{3} \rho$$

4.2. Boundary Conditions

Various forms of boundary conditions for the microflows have been presented recently. In the present work, the combination of bounce-back and specular reflection boundary condition (CBBSR) boundary scheme is employed in order to perceive the slip boundary conditions [29, 33]. For instance, the unknown distribution functions at $J=1$ (the bottom wall is plated at $J=0.5$) are given as:

$$\tilde{f}_2 = \tilde{f}_4 \quad (58)$$

$$\tilde{f}_5 = r_b \times \tilde{f}_7 + (1 - r_b) \times \tilde{f}_6$$

where \tilde{f}_i are the post-collision distribution functions at $J=1$, and $0 \leq r_b \leq 1$ is the portion of the bounce-back part in the combination of boundary conditions.

For isothermal rarefied gas flows, the widely used boundary condition for the Navier–Stokes equations is the second-order slip scheme [39]:

$$u_s = A_1 \sigma_v \lambda \left. \frac{\partial u}{\partial n} \right|_w - A_2 \lambda^2 \left. \frac{\partial^2 u}{\partial n^2} \right|_w \quad (59)$$

where u_s is the slip velocity, n is the unit vector normal to the wall, the subscript w denotes the quantity at the wall, and $\sigma_v = (2 - \sigma)/\sigma$, in which σ is the tangential momentum accommodation coefficient (TMAC). A_1 and A_2 are two parameters dependent on gas-solid interaction properties. In the literature, there are some suggestions for

A_1 and A_2 . e.g., $A_1 = 1.1466$ and $A_2 = 0.9756$ [31, 40]; $A_1 = 1.11$ and $A_2 = 0.61$ [9]; $A_1 = 1$ and $A_2 = 0.5$ [39].

The kinetic theory and molecular simulations displays that Maxwell's first order slip coefficient ($A_1 = 1$ and $A_2 = 0$) [41] sometimes suffers from a lack of accuracy and overestimates the amount of microscopic actual slip velocity. By employing an approximate method in the kinetic theory, Loyalka et al. suggested a modification of Maxwell's slip scheme. The proposed coefficient is $A_1 = 1 - 0.1817\sigma$ [42].

When the Bomanquet-type effective viscosity is applied, Equation (59) should be modified as:

$$u_s = B_1 \sigma_v \lambda_e \left. \frac{\partial u}{\partial n} \right|_w - B_2 \lambda_e^2 \left. \frac{\partial^2 u}{\partial n^2} \right|_w \quad (60)$$

where $\lambda_e = (\mu_e/p)\sqrt{\pi RT/2}$. Based on the modification of Maxwell's argument [42] $B_1 = 1 - 0.1817\sigma$ is selected. Some suggestions for coefficient B_2 through harmonizing slip scheme with the results of analytical and experimental flow rates [9] are 0.8 [31], 0.55 [33] and $(1/\pi) + (1/2)(\sigma_v B_1)^2$ [1]. Table 2. Summarizes these different values for wall-distance functions, slip coefficients and grid sizes.

In order to coordinate the second-order slip boundary condition at the macroscopic level, the parameter r_b and the relaxation rate s_q are selected as below [29, 31, 33, 43]

$$r_b = \left(1 + \sqrt{\frac{\pi}{6}} B_1 \sigma_v \right)^{-1} \quad (61)$$

$$s_q^{-1} = \frac{1}{2} + \frac{4\pi B_2 \left(s_v^{-1} - \frac{1}{2} \right)^2}{16 \left(s_v^{-1} - \frac{1}{2} \right)}$$

5. Results and Discussion

In this section, the Cascaded Lattice Boltzmann is applied to a microchannel gas flow. The abovementioned parameters a (Bomanquet parameter) and B_1 are selected, as stated before. Moreover, $B_2 = (1/\pi) + (1/2)(\sigma_v B_1)^2$ is chosen. It is the best fitting value for the solution of the linearized Boltzmann equation through investigations with different values of it. The other parameters are chosen as follows: $\delta x = \delta y = \delta t = 1$, $s_3 = 1.1$, $s_8 = 1.2$, $s_{4,5} = s_g$ and $s_{6,7} = s_q$. The stability criteria for the proposed CLBM is defined as below [44]:

$$\delta = \sqrt{\frac{1}{N} \sum_{i=1}^N (u^{n+1} - u^n)^2 + (v^{n+1} - v^n)^2} \leq 10^{-7} \quad (62)$$

Where N represents the whole nodes in the solution domain, n and $n+1$ are related to the present, and the previous time step and u and v are the velocity components in x and y directions, respectively. This criterion is satisfied for all cases studied here.

5.1. Microchannel with periodic boundary condition

Table 2. Various values for wall-distance functions, slip coefficients and grid sizes

Author(s)	Wall-distance function	B ₁	B ₂	Grid (Force B.C)	Grid (Pressure B.C)
Guo & Zheng [29]	-	1.1466	0.9757	16×31	-
Maxwell [41]	-	1	0	-	-
Hadjiconstantinou [9]	-	1.11	0.61	-	-
Kandlikar <i>et al.</i> [39]	-	1	0.5	-	-
Cercignani [40]	-	1.1466	0.9756	-	-
Loyalka <i>et al.</i> [42]	-	1-0.1817σ	0	-	-
Guo <i>et al.</i> [14]	Arctangent	-	-	-	2000×20
Li <i>et al.</i> [31]	Bosanquet	1-0.1817σ	0.8	50×50	2000×20
Liu & He [33]	Bosanquet	1-0.1817σ	0.55	50×50	2000×20
Liu & Guo [1]	Tang	1-0.1817σ	$(1/\pi)+(1/2)(\sigma_v B_1)^2$	-	2100×21
Present Work	Bosanquet	1-0.1817σ	$(1/\pi)+(1/2)(\sigma_v B_1)^2$	51×51	2100×21

First, the force-driven gaseous flow in a microchannel with periodic boundary conditions is inspected. This paper employs periodic boundary conditions at the inlet and outlet of the channel. Both channel walls are postulated in order to be completely diffusive ($\sigma = 1$), and the CBBSR scheme is employed in order to discern the second-order slip boundary condition, with its details in section 2.3. The constant driven force is implemented by setting $F_x=0.0001$.

5.1.1. Grid independency

The grid independence for the $Kn = 0.1128$ is contemplated here. The grid sizes of 21×21, 51×51, and 101×101 Lu are selected to compare. Figure 2 represents the streamwise velocity normalized by the average velocity at the outlet ($U=u/u_{ave}$) at different values of Kn . It can be observed that the results of the grids 51×51 and 101×101 Lu match well with each other. Therefore, the size of 51×51 is chosen for the present work.

5.1.2. Results of velocity profile

Figure 3 demonstrates normalized velocity at the outlet at different values of Kn . The results are compared with the previous works of the Linearized Boltzmann Equation acquired by Ohwada *et al.* [7], the conventional N-S solution applying a by Hadjiconstantinou [9], MRT results by Guo *et al.* [43], Filter-Matrix Lattice Boltzmann Method by Zhuo *et al.* [45] and the CLBM with constant

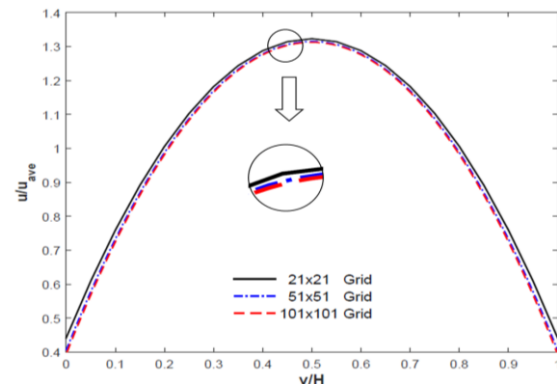


Figure 2. Normalized velocity at the outlet at different values of Kn .

Bosanquet factor by Li *et al.* [33]. It can be perceived that the N-S solutions significantly deviate from the Ohwada's Linearized Boltzmann Equation solutions almost in all ranges of Kn numbers. The MRT results also begin its deviation in the middle of the transitional flow regime ($Kn \geq 1.1284$). It is probably due to the difference in frames of reference between the CLBM and MRT. The results of the present work match better than CLBM with constant Bosanquet parameter with the Ohwada's solutions in almost all Kn numbers. The present results are comparable with the CLBM accompanying the constant Bosanquet parameter in estimating the streamwise velocity. This demonstrates the superiority of our suggestion for the nonconstant Bosanquet parameter. The

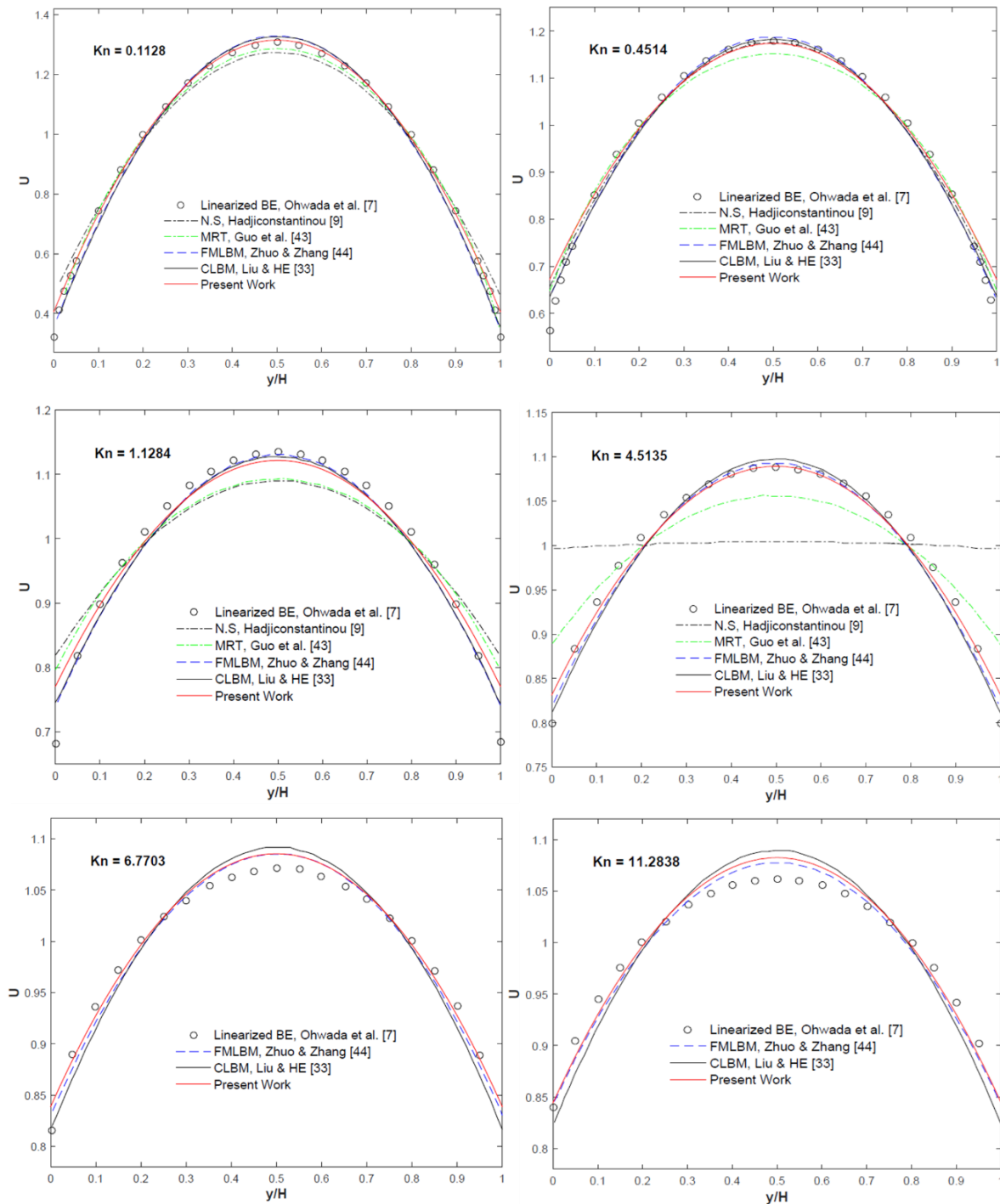


Figure 3. Streamwise velocity normalized by the average velocity at the outlet for fully diffusive walls with periodic boundary conditions driven by a constant force at different values of Kn .

present results are also better than the Filter-matrix Lattice Boltzmann Method results for most parts of the Kn regions; However, in the last third portion of the transitional flow regime ($Kn \geq 6.7703$), the present results slightly deviate from the Ohwada's solutions. It is noteworthy to mention that our results have some discrepancies between the present work and Ohwada's solutions in predicting the slip velocity, but they match better than the other works with the Ohwada's solutions across the channel.

For a more detailed comparison, Velocity contours and vectors for Knudsen numbers of 0.1128, 1.1284, and 11.2838 are portrayed in Figure 4, respectively, from left to right. In consonance with the figure, as the Knudsen number or the rarefaction effects increased, the velocity profiles get more smooth and uniform across the channel.

Figure 5 reveals the normalized volumetric flow rate against Kn number. The present results are compared with the linearized BE solutions by Cercignani *et al.* [46], the N-S solutions by Hadjiconstantinou [9], the MRT results

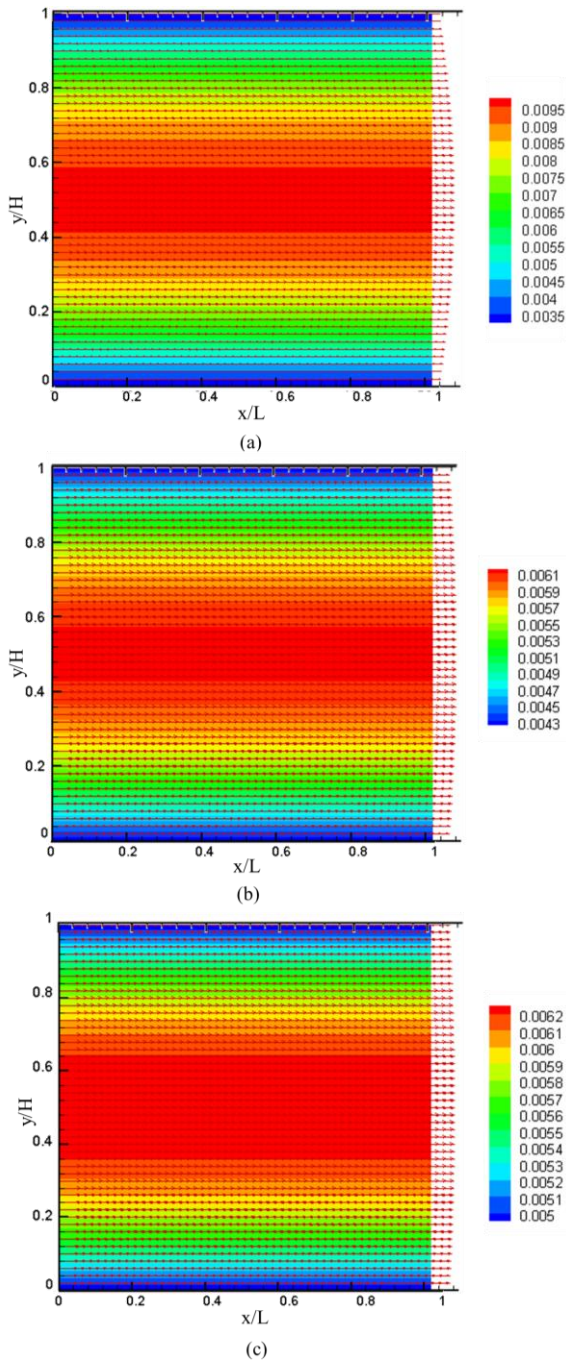


Figure 4. Velocity contours and vectors for Knudsen numbers of 0.1128 (a), 1.1284 (b), and 11.2838 (c).

by Guo *et al.* [43] and the CLBM with constant Bosanquet factor by Li *et al.* [33]. It can be observed that our results agree with other methods very well as $Kn < 0.5$. For larger Kn numbers, the prediction of the present method is a little larger than other methods, but the trend of the present results is the same as the other results. Furthermore, in the last portion of the transitional flow regime, the present work coordinates better than CLBM with constant Bosanquet parameter with the Cercignani's solutions. The error sum of squares between present results and the Cercignani's solutions for Kn numbers of 0.8 to 10 is 0.6091 while this error for CLBM with constant Bosanquet parameter is 0.6396.

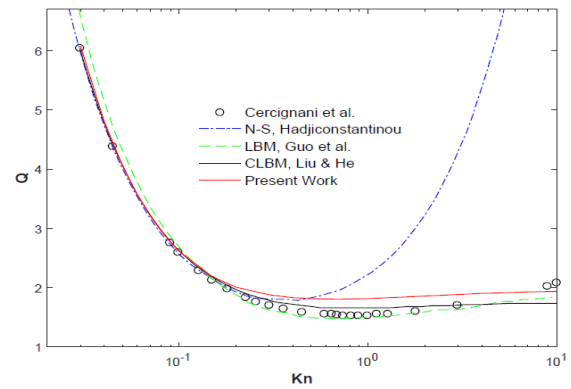


Figure 5. Normalized flow rate in a microchannel with periodic boundary condition driven by a constant force.

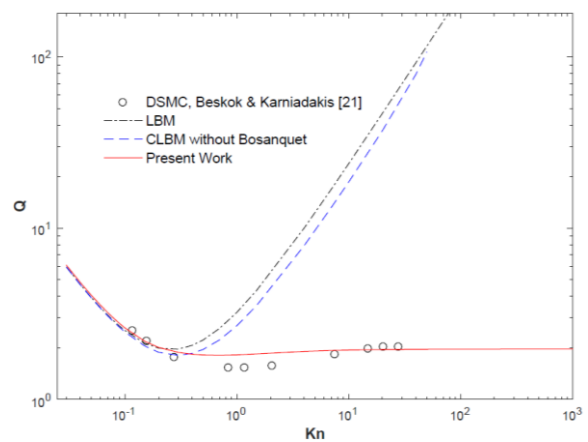


Figure 6. Normalized flow rate against Kn numbers from 0 to 1000.

Figure 5 also displays the well-known Knudsen minimum phenomenon, which occurs at about $Kn = 0.8$ for Cercignani's solution. The present work predicts this phenomenon at $Kn = 0.7$.

Figure 6 compares the present results, LBM and CLBM, without the Bosanquet parameter for the normalized flow rate against Kn numbers from almost 0 to 1000. Some computer codes are written for LBM and CLBM without the Bosanquet parameter. The ability of a model to catch the flow behavior in such high Kn numbers is obvious in the figure. The results are also compared with DSMC results presented by Beskok and Karniadakis [21], which proposed for Kn up to 50. Confirming to the figure, the results of LBM has a large deviation from the results of DSMC. Moreover, the CLBM model without the Bosanquet parameter gets unstable in $Kn = 70$, after its obvious deviation from the results of DSMC. The present CLBM with nonconstant Bosanquet parameter for boundary conditions works well for the widest range of Kn. This is due to the fact that the CLBM is more stable than previous versions of LBM. Consequently, it can predict flow behavior for higher Kn numbers.

5.2. Microchannel with pressure boundary condition

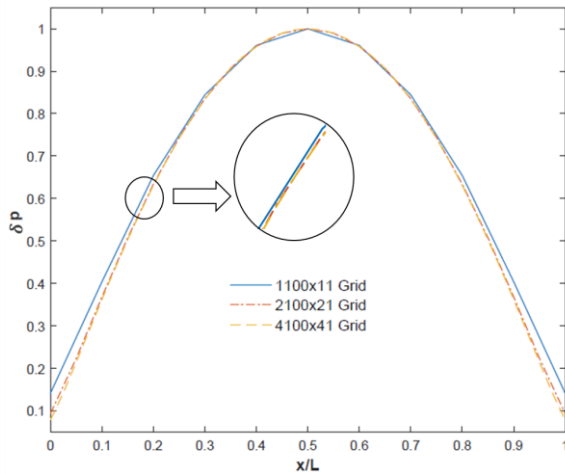


Figure 7. Pressure deviation from linear distribution along the microchannel.

In this section, the proposed CLBM is employed to the pressure-driven gaseous flow in a long microchannel with height $H = 1$ and length $L = 100$. The pressures are set to be p_{in} and p_{out} , respectively. The ratio of the length L to the height H of the channel is 100. The CBBSR boundary scheme is applied to the bottom and top walls of the channel. p_{in} and p_{out} are used for inlet and outlet pressure boundary conditions. The ratio of p_{in} and p_{out} takes 1.4 and 2 in our simulations. Three cases are inspected according to the Knudsen number at the exit, i.e., $Kn_{out}=0.0194$, 0.194, and 0.388.

5.2.1. Grid independency

The grid independence for the $Kn_{out} = 0.0194$ and pressure ratio (PR=1.4) is deliberated here. The sizes of the grids to compare are 1100×11 , 2100×21 , and 4100×41 . Figure 7 exhibits the normalized pressure deviation from its linear distribution in conformity with the microchannel p_l , $\delta p = \frac{p - p_l}{p_{out}}$. In consonance to the figure, the results of the grids 2100×21 and 4100×41 are very close to each other. Therefore, the grid size of 2100×21 is a reasonable choice for the present work.

5.2.2. Results of velocity profile and pressure distribution

In the Figures 8, 9 and 10, the deviation of pressure from its linear and the normalized streamwise velocity u/u_{max} at the outlet are compared with the slip N-S solutions by Arkilic *et al.* [8], the DSMC and information-preservation DSMC (IP-DSMC) results of Shen *et al.* [47] and the CLBM with constant Bomanquet factor by Li *et al.* [33]. It can be seen that the results of the present work are in good agreement with the benchmark data in the literature. The proposed CLBM also has better results than the previous one in all three cases. The profiles of the velocity and pressure deviation acquired by the proposed CLBM agree well with the DSMC, IP-DSMC, and slip N-S solutions. However, a small discrepancy in the velocity is still observed near the two walls as a result to the Knudsen layer effect. Figure 10 clearly indicates significant improvements made by the present model for

$Kn_{out} = 0.388$ and $p_{in}=2$ (the slip flow regime). This is the region that previous works have an obvious deviation from the results of DSMC and IP-DSMC in it. Again, it displays superiority of the present CLBM in one of the most major applications of MEMS. The effect of selecting a nonconstant Bomanquet parameter becomes consequential in this region. Figure 11 persuades the pressure contour for $Kn=0.388$.

Here, the velocity profile of the present CLBM is in good agreement with the DSMC and IP-DSMC results. The pressure deviation profile of our work has some discrepancies; however, it matches far more with them in comparison with the CLBM with constant Bomanquet parameter.

The other major parameter in a microchannel is the slip velocity. It can be observed from figures 8 to 10 that the CLBM with constant Bomanquet parameter has a better prediction for slip velocity than the present work. The reason for this dissimilarity is that this paper does not employ a consistent linear extrapolation scheme for inlet and outlet boundary conditions.

Figure 12 depicts the normalized flow rate against the average Knudsen number (Kn_m). Confirming to the figure, the present results are in good agreement with the benchmark results [7, 28, 48] for most of the Kn_m s. For larger Kn_m s there are some discrepancies between our model and these solutions. The reason here may be that the solutions of the Boltzmann equation of Cercignani *et al.* [28] and Ohwada *et al.* [7] assumed a linear pressure distribution along the channel and the pressure ratio between the inlet and outlet is very small. These may be the reasons for the small discrepancy between the present CLBM and these solutions. However, the proposed CLBM indicates a clear improvement in predicting the mass flow rate for LBE Methods.

Conclusion

In this paper, a Cascaded Lattice Boltzmann Method with a nonconstant Bomanquet parameter model was developed in order to investigate microchannel gas flows in the slip and transition flow regimes with a wide range of Knudsen numbers. The CBBSR boundary scheme with a second-order slip boundary condition was applied. The nonlinearity of Knudsen number in accordance with the channel and the effects of wall confinement are deliberated as well. This paper suggested applying the nonconstant Bomanquet parameter instead of the constant one. The constant-force-driven and pressure-driven flow microchannel were simulated under different conditions. The velocity profile, pressure distribution, and mass flow rate were inspected, and the results were in good agreement with the benchmark solutions and experimental data reported in the literature. The proposed CLBM reveals a clear improvement in predicting the flow behaviors of microchannel gas flows for the previous classic and CLBMs. The Knudsen minimum phenomenon was also well captured by the present model. The main

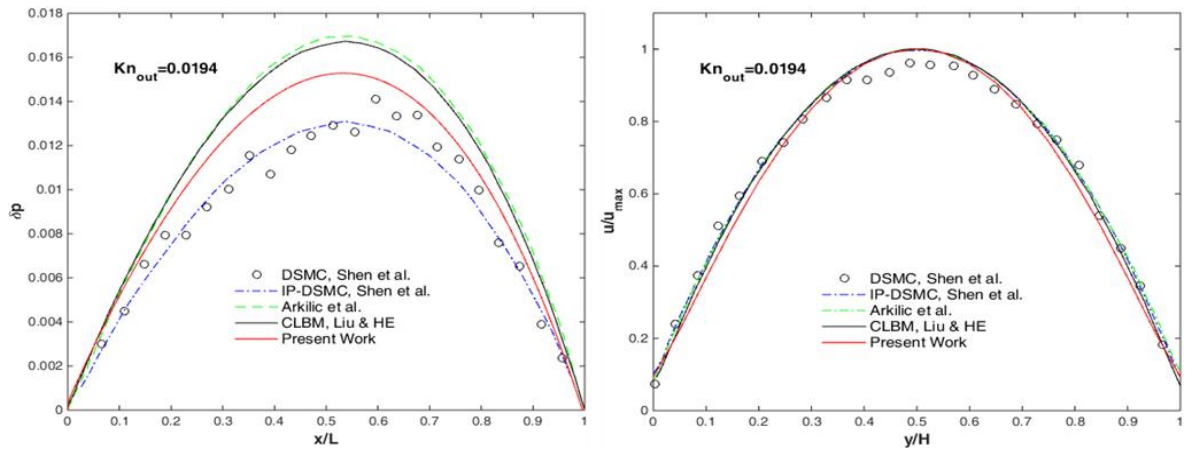


Figure 8. Pressure deviation along the channel (Left), and u- velocity at the outlet (Right). $Kn_{out} = 0.0194$, $p_{in}/p_{out} = 1.4$.

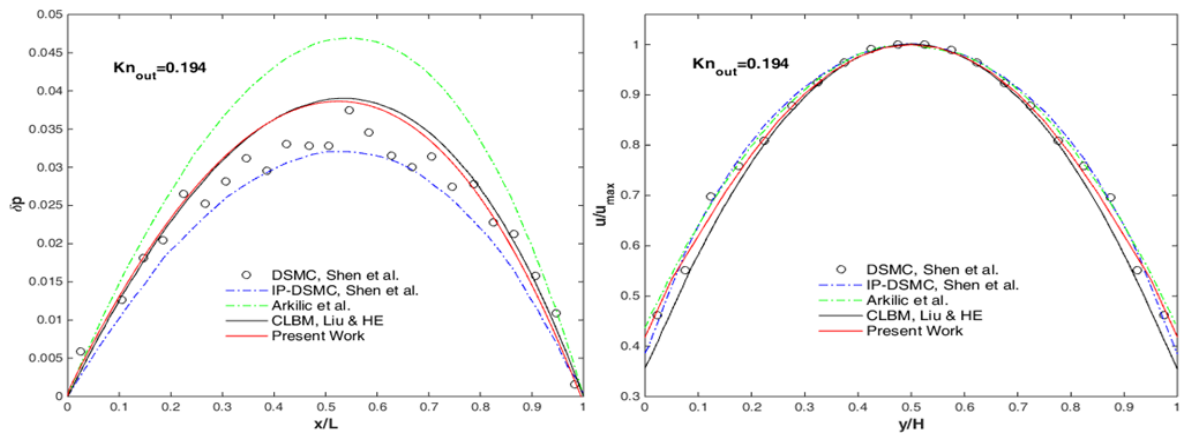


Figure 9. Pressure deviation along the channel (Left), and u- velocity at the outlet (Right). $Kn_{out} = 0.194$, $p_{in}/p_{out} = 2$.

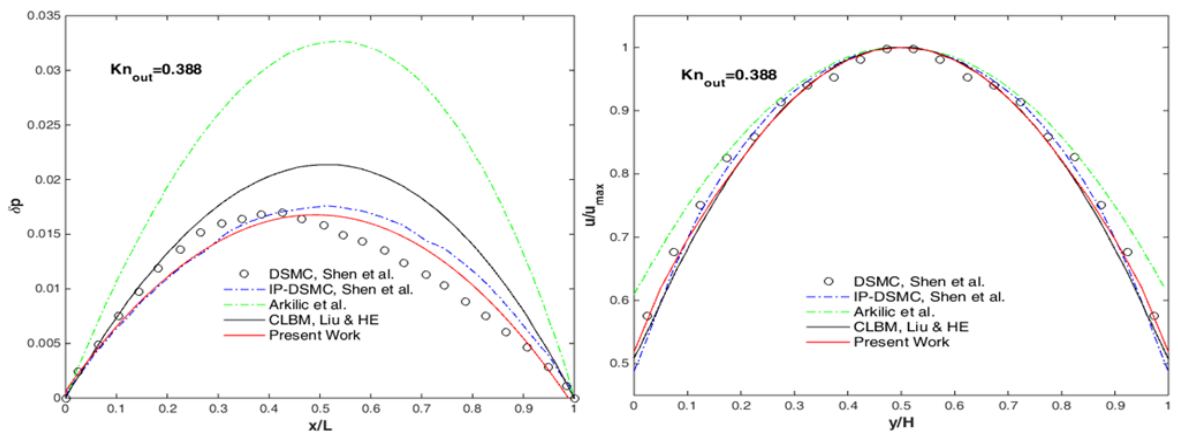


Figure 10. Pressure deviation along the channel (Left), and u- velocity at the outlet (Right). $Kn_{out} = 0.388$, $p_{in}/p_{out} = 2$.

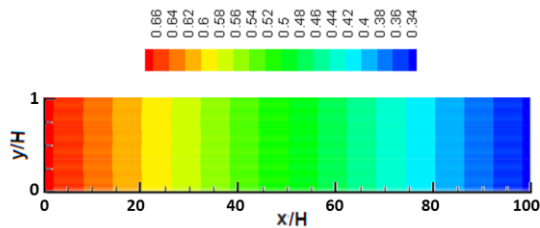


Figure 11. Pressure contour for $Kn=0.388$ in a microchannel with pressure boundary conditions.

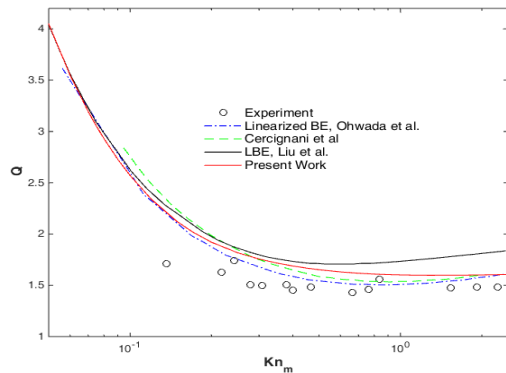


Figure 12. Normalized mass flow rates for different average Knudsen number.

findings of this paper are summarized as below:

- The proposed CLBM indicates a clear improvement in predicting the flow behaviors of microchannel gas flows for the previous classic and CLBM.
- The proposed CLBM can be applied for the widest range of Knudsen number.
- For the first time, the effect of wall confinement is considered employing a function with the nonconstant Bomanquet parameter as a substitute for the constant one.
- The results of the proposed model are in good agreement with the benchmark solutions and the experimental data reported in the literature
- The Knudsen minimum phenomenon was also well captured by the proposed model.

Nomenclature

All variable using this manuscript, listed in nomenclature.

λ	Mean free path
λ_e	Effective mean free path
L	Length of channel
H	Height of channel
Kn	Knudsen number
Kn_{out}	Knudsen number at the outlet
e_i	Velocity field
c	Speed in lattice units
cs	Speed in lattice units
t	Time
x	Position in coordinate system

∂t	Discrete time step
∂x	Lattice
τ_s	Relaxation time
f_i	Particle density distribution function
f_{ieq}	Equilibrium density distribution function
ρ	Density of fluid
μ	Dynamic viscosity of fluid
μ_e	Effective viscosity
F	Body force term
K	orthogonal transformation matrix
s_i	Relaxation rate
s_θ	Shear viscosity relaxation rate
s_b	Bulk viscosity relaxation rate
s_q	Relaxation rate of third order moments
ν	Kinematic viscosity of fluid
u	Streamwise velocity
v	Normal velocity
U	Average velocity
w	Weight coefficient
P	Pressure
P_{in}	Pressure at the inlet
P_{out}	Pressure at the outlet
R	Universal gas constant
Ψ	Wall-distance function
T	Temperature
a	Bomanquet Parameter
t	Tangential direction
n	Normal direction
κ	Central velocity moment
κ'	Raw velocity moment
Ω	Collision operator
S	Source term
g	Collision kernel
T	non-orthogonal transformation matrix
u_s	slip velocity
w	Quantity at the wall
σ_v	Tangential momentum accommodation coefficient
A_i	Coefficients of second order slip boundary conditions
B_i	Modified coefficients of second order boundary conditions
r_b	The portion of the bounce-back part in the combination of boundary conditions

Acknowledgements

The authors acknowledge Professor Kannan N. Premnath, the professor in the Department of Chemical Engineering, University of California, for the help in programming CLBM.

References

- [1] AGRAWAL, A., DJENIDI, L. & AGRAWAL, A. 2009. Simulation of gas flow in microchannels with a single 90 bend. *Computers & Fluids*, 38, 1629-1637.
- [2] AHMED, I. & BESKOK, A. 2002. Rarefaction, compressibility, and viscous heating in gas microfilters. *Journal of Thermophysics and Heat Transfer*, 16, 161-170.
- [3] ARKILIC, E. B., SCHMIDT, M. A. & BREUER, K. S. 1997. Gaseous slip flow in long microchannels. *Journal of Microelectromechanical systems*, 6, 167-178.
- [4] ASADOLLAHI, A., RASHIDI, S. & ESFAHANI, J. A. 2017. Condensation process and phase-change in the presence of obstacles inside a minichannel. *Meccanica*, 52, 2265-2274.
- [5] ASADOLLAHI, A., RASHIDI, S. & MOHAMAD, A. A. 2018. Removal of the liquid from a micro-object and controlling the surface wettability by using a rotating shell-Numerical simulation by Lattice-Boltzmann method. *Journal of Molecular Liquids*, 272, 645-655.
- [6] BECK, C. & ROEPSTORFF, G. 1990. From stochastic processes to the hydrodynamic equations. *Physica A: Statistical Mechanics and its Applications*, 165, 270-278.
- [7] BESKOK, A. & KARNIADAKIS, G. E. 1999. Report: a model for flows in channels, pipes, and ducts at micro and nano scales. *Microscale Thermophysical Engineering*, 3, 43-77.
- [8] BHATNAGAR, P. L., GROSS, E. P. & KROOK, M. 1954. A model for collision processes in gases. I. Small amplitude processes in charged and neutral one-component systems. *Physical review*, 94, 511.
- [9] CERCIGNANI, C. 1964. Higher order slip according to the linearized Boltzmann equation. CALIFORNIA UNIV BERKELEY INST OF ENGINEERING RESEARCH.
- [10] CERCIGNANI, C. 1969. *Mathematical methods in kinetic theory*, Springer.
- [11] CERCIGNANI, C. & DANERI, A. 1963. Flow of a rarefied gas between two parallel plates. *Journal of Applied Physics*, 34, 3509-3513.
- [12] CERCIGNANI, C., LAMPIS, M. & LORENZANI, S. 2004. Variational approach to gas flows in microchannels. *Physics of Fluids*, 16, 3426-3437.
- [13] DUBOIS, F., FEVRIER, T. & GRAILLE, B. 2015a. Lattice Boltzmann schemes with relative velocities. *Communications in Computational Physics*, 17, 1088-1112.
- [14] DUBOIS, F., FÉVRIER, T. & GRAILLE, B. 2015b. On the stability of a relative velocity lattice Boltzmann scheme for compressible Navier–Stokes equations. *Comptes Rendus Mécanique*, 343, 599-610.
- [15] FEI, L. & LUO, K. H. 2017. Consistent forcing scheme in the cascaded lattice Boltzmann method. *Physical Review E*, 96, 053307.
- [16] GEIER, M., GREINER, A. & KORVINK, J. 2009. A factorized central moment lattice Boltzmann method. *The European Physical Journal Special Topics*, 171, 55-61.
- [17] GEIER, M., GREINER, A. & KORVINK, J. G. 2006. Cascaded digital lattice Boltzmann automata for high Reynolds number flow. *Physical Review E*, 73, 066705.
- [18] GUO, Z., ZHAO, T. & SHI, Y. 2006. Physical symmetry, spatial accuracy, and relaxation time of the lattice Boltzmann equation for microgas flows. *Journal of Applied physics*, 99, 074903.
- [19] GUO, Z. & ZHENG, C. 2008. Analysis of lattice Boltzmann equation for microscale gas flows: relaxation times, boundary conditions and the Knudsen layer. *International Journal of Computational Fluid Dynamics*, 22, 465-473.
- [20] GUO, Z., ZHENG, C. & SHI, B. 2008. Lattice Boltzmann equation with multiple effective relaxation times for gaseous microscale flow. *Physical Review E*, 77, 036707.
- [21] HADJICONSTANTINO, N. G. 2003. Comment on Cercignani's second-order slip coefficient. *Physics of Fluids*, 15, 2352-2354.
- [22] HOMAYOON, A., ISFAHANI, A. M., SHIRANI, E. & ASHRAFIZADEH, M. 2011. A novel modified lattice Boltzmann method for simulation of gas flows in wide range of Knudsen number. *International Communications in Heat and Mass Transfer*, 38, 827-832.
- [23] HOSSEINI, R., RASHIDI, S. & ESFAHANI, J. A. 2017. A lattice Boltzmann method to simulate combined radiation-force convection heat transfer mode. *Journal of the Brazilian Society of Mechanical Sciences and Engineering*, 39, 3695-3706.
- [24] KANDLIKAR, S., GARIMELLA, S., LI, D., COLIN, S. & KING, M. R. 2005. Heat transfer and fluid flow in minichannels and microchannels, elsevier.
- [25] LECLAIRE, S., PELLERIN, N., REGGIO, M. & TRÉPANIÉ, J.-Y. 2014. Multiphase flow modeling of spinodal decomposition based on the cascaded lattice Boltzmann method. *Physica A: Statistical Mechanics and its Applications*, 406, 307-319.
- [26] LEE, T. & LIN, C.-L. 2005. Rarefaction and compressibility effects of the lattice-Boltzmann-equation method in a gas microchannel. *Physical Review E*, 71, 046706.

- [27] LI, Q., HE, Y., TANG, G. & TAO, W. 2011. Lattice Boltzmann modeling of microchannel flows in the transition flow regime. *Microfluidics and nanofluidics*, 10, 607-618.
- [28] LIU, Q. & HE, Y.-L. 2016. Numerical modelling of microchannel gas flows in the transition flow regime using the cascaded lattice Boltzmann method. *arXiv preprint arXiv:1603.01955*.
- [29] LIU, X. & GUO, Z. 2013. A lattice Boltzmann study of gas flows in a long micro-channel. *Computers & Mathematics with Applications*, 65, 186-193.
- [30] LOCKERBY, D. A., REESE, J. M. & GALLIS, M. A. 2005. The usefulness of higher-order constitutive relations for describing the Knudsen layer. *Physics of Fluids*, 17, 100609.
- [31] LOPEZ, P. 2014. Thermal Lattice Boltzmann Simulation for Rarefied Flow in Microchannels.
- [32] LOYALKA, S., PETRELLIS, N. & STORVICK, T. 1975. Some numerical results for the BGK model: Thermal creep and viscous slip problems with arbitrary accommodation at the surface. *The Physics of Fluids*, 18, 1094-1099.
- [33] LYCETT-BROWN, D. & LUO, K. H. 2014. Multiphase cascaded lattice Boltzmann method. *Computers & Mathematics with Applications*, 67, 350-362.
- [34] LYCETT-BROWN, D., LUO, K. H., LIU, R. & LV, P. 2014. Binary droplet collision simulations by a multiphase cascaded lattice Boltzmann method. *Physics of Fluids*, 26, 023303.
- [35] MAXWELL, J. C. 1879. VII. On stresses in rarified gases arising from inequalities of temperature. *Philosophical Transactions of the royal society of London*, 231-256.
- [36] MICHALIS, V. K., KALARAKIS, A. N., SKOURAS, E. D. & BURGANOS, V. N. 2010. Rarefaction effects on gas viscosity in the Knudsen transition regime. *Microfluidics and nanofluidics*, 9, 847-853.
- [37] MOHAMAD, A. A. 2011. *Lattice Boltzmann method: fundamentals and engineering applications with computer codes*, Springer Science & Business Media.
- [38] NING, Y., PREMNATH, K. N. & PATIL, D. V. 2016. Numerical study of the properties of the central moment lattice Boltzmann method. *International Journal for Numerical Methods in Fluids*, 82, 59-90.
- [39] NIU, X., SHU, C. & CHEW, Y. 2004. A lattice Boltzmann BGK model for simulation of micro flows. *EPL (Europhysics Letters)*, 67, 600.
- [40] OHWADA, T., SONE, Y. & AOKI, K. 1989. Numerical analysis of the Poiseuille and thermal transpiration flows between two parallel plates on the basis of the Boltzmann equation for hard-sphere molecules. *Physics of Fluids A: Fluid Dynamics*, 1, 2042-2049.
- [41] PREMNATH, K. N. & BANERJEE, S. 2009. Incorporating forcing terms in cascaded lattice Boltzmann approach by method of central moments. *Physical Review E*, 80, 036702.
- [42] RAHMATI, A. R. & NIAZI, S. 2015. Application and Comparison of Different Lattice Boltzmann Methods on Non-Uniform Meshes for Simulation of Micro Cavity and Micro Channel Flow. *Journal of Computational Methods In Engineering*, 34, 97-118.
- [43] SHEN, C., TIAN, D.-B., XIE, C. & FAN, J. Examination of the LBM in simulation of microchannel flow in transitional regime. *ASME 2003 1st International Conference on Microchannels and Minichannels*, 2003. American Society of Mechanical Engineers, 405-410.
- [44] SHOKOUHMAND, H. & ISFAHANI, A. M. 2011. An improved thermal lattice Boltzmann model for rarefied gas flows in wide range of Knudsen number. *International communications in heat and mass transfer*, 38, 1463-1469.
- [45] STOPS, D. 1970. The mean free path of gas molecules in the transition regime. *Journal of Physics D: Applied Physics*, 3, 685.
- [46] TANG, G., ZHANG, Y., GU, X. & EMERSON, D. 2008. Lattice Boltzmann modelling Knudsen layer effect in non-equilibrium flows. *EPL (Europhysics Letters)*, 83, 40008.
- [47] ZHANG, Y.-H., GU, X.-J., BARBER, R. W. & EMERSON, D. R. 2006. Capturing Knudsen layer phenomena using a lattice Boltzmann model. *Physical Review E*, 74, 046704.
- [48] ZHUO, C. & ZHONG, C. 2013. Filter-matrix lattice Boltzmann model for microchannel gas flows. *Physical Review E*, 88, 053311.